arXiv:1404.6211v1 [cond-mat.quant-gas] 24 Apr 2014

Spin-orbit-coupled topological Fulde-Ferrell states of fermions in a harmonic trap

Lei Jiang[1], Eite Tiesinga[1], Xia-Ji Liu[2], Hui Hu[2] and Han Pu[3]
[1] *Joint Quantum Institute, University of Maryland and National Institute of Standards and Technology, Gaithersburg, Maryland 20899, USA*
[2] *Centre for Atom Optics and Ultrafast Spectroscopy, Swinburne University of Technology, Melbourne 3122, Australia*
[3] *Department of Physics and Astronomy, and Rice Quantum Institute, Rice University, Houston, Texas 77251, USA*
(Dated: April 25, 2014)

Motivated by recent experimental breakthroughs in generating spin-orbit coupling in ultracold Fermi gases using Raman laser beams, we present a systematic study of spin-orbit-coupled Fermi gases confined in a quasi-one-dimensional trap in the presence of an in-plane Zeeman field (which can be realized using a finite two-photon Raman detuning). We find that a topological Fulde-Ferrell state will emerge, featuring finite-momentum Cooper pairing and zero-energy Majorana excitations localized near the edge of the trap based on the self-consistent Bogoliubov-de Genes (BdG) equations. We find analytically the wavefunctions of the Majorana modes. Finally using the time-dependent BdG we show how the finite-momentum pairing field manifests itself in the expansion dynamics of the atomic cloud.

PACS numbers: 03.75.Ss, 05.30.Fk, 03.65.Vf, 67.85.Lm

Over the past few years, spin-orbit coupled quantum gases have received a great amount of interest in both the cold atom and condensed matter communities [1–12]. This can be largely attributed to the fact that such a system can potentially realize exotic quantum phases in a controlled fashion. So far only one type of spin-orbit coupling (SOC) — the equal-weight Rashba and Dresselhaus SOC — has been realized [13, 14], although several theoretical schemes have been proposed to realize more general types of SOC. Nevertheless, the experimentally realized SOC has already been shown to give rise to several interesting quantum phases. These include the topological superfluid phase in a one-dimensional (1D) system supporting Majorana modes near the boundaries [15–18], and the Fulde-Ferrell (FF) superfluid state featuring finite-momentum Cooper pairing [19–25]. Furthermore, in a 1D setting, these two features can coexist where one realizes an exotic topological FF superfluid [26–30]. Early experiments explored the possibility of the Fulde-Ferrell-Larkin-Ovchinnikov state in spin-imbalanced cold atoms [31–33], with indirect evidence only coming from a quasi-1D setup [34].

Previous work on topological FF phases focused on homogeneous 1D gases. In this work, we consider a system in a realistic 1D harmonic trapping potential and investigate how signatures of exotic phases can be probed in practice. Such a quasi-1D system can be realized by confining atoms in strong 2D optical lattices [34]. The presence of a trapping potential suppresses quantum fluctuations and makes mean-field calculations qualitatively reliable [35, 36]. The two goals of this work are: (1) We show how a Majorana mode, the smoking gun of the topological order, manifests itself in the density of states (DOS) in both real and momentum space. We obtain the wavefunctions of the Majorana quasi-particle states analytically and show that they are in good agreement with numerical results based on the Bogoliubov-de Gennes (BdG) formalism. (2) We show how finite-momentum Cooper pairing, the telltale signal of the FF phase, leaves detectable traces in the expansion dynamics of the atomic cloud.

Model — We consider a spin-1/2 Fermi gas confined in a 1D harmonic trap. Its Hamiltonian is given by $H = H_0 + H_{\rm int}$, with single-particle component H_0 and interacting component $H_{\rm int}$ describing the s-wave contact interaction. In fact

$$
\begin{aligned}
H_0 &= \int dx\, \psi_\uparrow^\dagger(x)[H_s + \delta/2]\psi_\uparrow(x) + \int dx\, \psi_\downarrow^\dagger(x)[H_s - \delta/2]\psi_\downarrow(x) - \frac{\Omega_R}{2}\int dx\, \left[\psi_\uparrow^\dagger(x) e^{i2k_R x}\psi_\downarrow(x) + H.c.\right] \\
H_{\rm int} &= g_{1D}\int dx\, \psi_\uparrow^\dagger(x)\psi_\downarrow^\dagger(x)\psi_\downarrow(x)\psi_\uparrow(x),
\end{aligned}
$$

where $\psi_\uparrow(x)$, $\psi_\downarrow(x)$ are Fermi annihilation operators for the two spin states. The Hamiltonian $H_s = -\frac{\hbar^2}{2m}\frac{\partial^2}{\partial x^2} - \mu + V_T(x)$ with μ being the chemical potential and $V_T(x) = \frac{1}{2}m\omega^2 x^2$ the harmonic trapping potential with

a frequency ω. The constants δ and Ω_R represent the detuning and strength of the two-photon Raman coupling, respectively, $2\hbar k_R$ is the photon recoil momentum imparted to the atoms from the Raman lasers, and $\hbar$ is reduced Planck constant. Finally, g_{1D} is the 1D two-body s-wave interaction strength.

After applying the local gauge transformation

$$\begin{aligned}\psi_\uparrow(x) &= e^{ik_R x}\left[\phi_\uparrow(x) - i\phi_\downarrow(x)\right]/\sqrt{2}\,,\\ \psi_\downarrow(x) &= e^{-ik_R x}\left[\phi_\uparrow(x) + i\phi_\downarrow(x)\right]/\sqrt{2}\,,\end{aligned}$$

the single-particle Hamiltonian H_0 becomes

$$H_0 = \int dx\, \phi^\dagger[H_s + (-i\lambda\partial_x + \nu)\sigma_y - h\sigma_z]\,\phi\,, \quad (1)$$

where $\phi = [\phi_\uparrow(x), \phi_\downarrow(x)]^T$ and we have dropped a constant corresponding to the atomic recoil energy. In writing Eq. (1), we have defined the spin-orbit-coupling constant $\lambda \equiv \hbar^2 k_R/m$, the effective out-of-plane Zeeman field $h \equiv \Omega_R/2$ and the effective in-plane Zeeman field $\nu \equiv \delta/2$. It is convenient to define effective Zeeman field strength $b \equiv \sqrt{h^2+\nu^2}$. The operators σ_y and σ_z are Pauli matrices in the atomic spin basis. The interaction Hamiltonian $H_{\rm int}$ is invariant under this gauge transformation.

Bogoliubov-de Gennes formalism — In the mean-field BdG approximation, we assume a non-zero complex order parameter or gap $\Delta(x) \equiv -g_{1D}\langle\phi_\downarrow(x)\phi_\uparrow(x)\rangle = -ig_{1D}\langle\psi_\downarrow(x)\psi_\uparrow(x)\rangle$, and in terms of the Nambu spinor $\Phi(x) = [\phi_\uparrow(x), \phi_\downarrow(x), \phi_\uparrow^+(x), \phi_\downarrow^+(x)]^T$ the mean-field Hamiltonian becomes

$$H_{\rm mf} = \frac{1}{2}\int dx\, \Phi^\dagger(x) H_{\rm BdG}\Phi(x) + {\rm Tr}[H_s] - \int dx\, \frac{|\Delta(x)|^2}{g_{1D}}\,,$$

where

$$H_{\rm BdG} = \begin{bmatrix} H_s - h & -\lambda\partial_x - i\nu & 0 & -\Delta(x) \\ \lambda\partial_x + i\nu & H_s + h & \Delta(x) & 0 \\ 0 & \Delta^*(x) & -H_s + h & \lambda\partial_x - i\nu \\ -\Delta^*(x) & 0 & -\lambda\partial_x + i\nu & -H_s - h \end{bmatrix}.$$

The Bogoliubov quasi-particles are obtained by diagonalizing

$$H_{\rm BdG}\,\varphi_\eta(x) = E_\eta\,\varphi_\eta(x)\,, \quad (2)$$

with energies E_η and wavefunctions $\varphi_\eta(x) = [u_{\uparrow\eta}(x), u_{\downarrow\eta}(x), v_{\uparrow\eta}(x), v_{\downarrow\eta}(x)]^T$ indexed by subscript $\eta = 1, 2, 3\ldots$ The wavefunctions are normalized such that $\sum_{\sigma=\uparrow,\downarrow}\int dx(|u_{\sigma\eta}(x)|^2 + |v_{\sigma\eta}(x)|^2) = 1$. The order parameter

$$\Delta(x) = -\frac{g_{1D}}{2}\sum_\eta\left[u_{\uparrow\eta}v_{\downarrow\eta}^* f(E_\eta) + u_{\downarrow\eta}v_{\uparrow\eta}^* f(-E_\eta)\right]$$

must be solved self consistently, where $f(E)$ is Fermi-Dirac distribution function $f(E) = 1/[e^{E/k_BT}+1]$ and T is the temperature. Here we present results for $T = 0$.

To solve the eigenvalue problem, we use the discrete variable representation of the plane wave basis [37]. We employ 1001 plane-wave bases and the total number of atoms is $N = 60$. In the harmonic trap with frequency ω, we define the non-interacting Fermi energy $E_F = \hbar\omega N/2$, the Fermi wave number k_F, obtained from $E_F = \hbar^2 k_F^2/(2m)$, and the Thomas-Fermi radius $x_{\rm TF} = \sqrt{N\hbar/(m\omega)}$. Throughout we use E_F and x_{TF} as the natural energy and length scale, respectively. Equation (2) is solved by using a "hybrid" method of Ref. [36, 38]. We start with an initial guess of the order parameter. We then find all the eigenpairs of $H_{\rm BdG}$ with energy $|E| \leqslant E_c$ where E_c is a cut-off energy that is chosen to be large compared to the Fermi energy but small compared to the full spectral width of the discretized $H_{\rm BdG}$. Typically we take $E_c = 8E_F$. For states above the energy cut-off, we employ a semi-classical method based on the local density approximation. The updated order parameter is calculated by combining the contributions from the numerical and semi-classical solutions. The procedure is repeated until convergence of the order parameter is reached.

It is convenient to characterize the interaction strength g_{1D} by a dimensionless interaction parameter $\gamma \equiv -mg_{1D}/(\hbar^2 n_0)$ which represents the ratio between the interaction and kinetic energy. Here $n_0 = (2/\pi)\sqrt{Nm\omega/\hbar}$ is the total atomic density at the trap center in the Thomas-Fermi approximation.

To study expansion dynamics, we solve the time-dependent BdG equation [39–42]

$$i\hbar\partial_t\,\varphi_\eta(x,t) = H_{\rm BdG}\,\varphi_\eta(x,t)\,,$$

with the initial wavefunction of $\varphi_\eta(x,0)$ set by the ground state of the trapped system obtained from Eq. (2). We use the Runge–Kutta method for the time propagation. The kinetic energy and the spin-orbit coupling term are propagated in the interaction picture using a fast Fourier transform.

Topological FF state in trap — In Fig. 1, we characterize the properties of the topological FF state in the trapped system using experimentally relevant parameters. Figure 1(a) shows atom density profiles of both spin species, $n_\sigma(x) = \langle\psi_\sigma^\dagger(x)\psi_\sigma(x)\rangle$, along with the magnitude of the order parameter $|\Delta(x)|$. The densities peak at the center of the trap, while $|\Delta(x)|$ has a minimum at the center and reaches its maximum value near the edge of the cloud. This is due to a peculiar property of 1D quantum gases [36]: for sufficiently large density, the effect of the interaction and thus the order parameter is enhanced by reducing the number density, while near the edge of the cloud, the order parameter has a power law dependence on density.

For positive two-photon detuning $\delta = 2\nu$ used in the calculation, the effective chemical potential for spin-up atoms, $\mu - \delta/2$, is lower than that for spin-down atoms,

$\mu + \delta/2$. Consequently, spin-up (spin-down) represents the minority (majority) species. As we change the sign of δ, the density profiles of the two spin species switch. This follows from a symmetry of the BdG Hamiltonian for this system: Under the simultaneous transformation $\nu \to -\nu$, $\Delta(x) \to -\Delta(-x)$ and

$$[u_{\uparrow\eta}(x),\, u_{\downarrow\eta}(x),\, v_{\uparrow\eta}(x),\, v_{\downarrow\eta}(x)] \to$$
$$[u_{\uparrow\eta}(-x),\, -u_{\downarrow\eta}(-x),\, v_{\uparrow\eta}(-x),\, -v_{\downarrow\eta}(-x)]\,,$$

Equation (2) remains invariant.

Figure 1(b) shows the real and imaginary parts of the order parameter. Near the center of the trap, the order parameter has the plane-wave form $\Delta(x) \simeq \Delta_0\, e^{iqx}$, indicating finite-momentum pairing. This is the characteristic signature of a FF superfluid state [43, 44]. The pairing momentum q can be easily extracted from the data. The inset of Fig. 1(b) shows that q increases nearly linearly as a function of ν.

Majorana modes — In Fig. 1(c), we show the low-lying quasi-particle excitation spectrum of the system. The two dots with zero energy are the Majorana modes characterizing the nontrivial topological nature of the system. The Majorana modes exist inside a gap in the energy spectrum. For comparison, a spectrum for a topologically trivial system is shown in the inset, where no states inside the gap exist. The wavefunctions of the two Majorana modes are plotted in Fig. 1(d). The two Majorana modes are spatially localized near the two edges of the cloud at $x = \pm x_{TF}$. Their wavefunctions satisfy the condition $|u_\sigma| = |v_\sigma|$. The contribution of the Majorana modes to the order parameter is negligible. This is not surprising as many states contribute to $\Delta(x)$.

Figure 2 shows the density of states both in real space and momentum space and defined by

$$\rho(x,\omega) = \frac{1}{2}\sum_{\sigma\eta}[|u_{\sigma\eta}|^2\delta(\omega - E_\eta) + |v_{\sigma\eta}|^2\delta(\omega + E_\eta)]\,,$$
$$\tilde{\rho}(k,\omega) = \frac{1}{2}\sum_{\sigma\eta}[|\tilde{u}_{\sigma\eta}|^2\delta(\omega - E_\eta) + |\tilde{v}_{\sigma\eta}|^2\delta(\omega + E_\eta)]\,,$$

where $\tilde{u}_{\sigma\eta}(k) = \int u_{\sigma\eta}(x)e^{ikx}dx$, $\tilde{v}_{\sigma\eta}(k) = \int v_{\sigma\eta}(x)e^{ikx}dx$ are the Fourier transforms of $u_{\sigma\eta}(x)$ and $v_{\sigma\eta}(x)$, respectively. In the calculations, the Dirac δ-function is replaced by a Gaussian with width on the order of spacings in the energy spectrum away from the gap. The zero-energy Majorana modes in the plots of the density of states are easily identified. They are localized in both real space (near $\pm x_{TF}$) and momentum space (around $k = 0$). In principle, the density of states can be measured in experiment by using spatial and momentum resolved radio-frequency spectroscopy [45].

We can derive analytic formulas for the Majorana wavefunctions using the fact that they are localized in both real and momentum spaces. The derivation with details found in the Supplemental Material [46] is based on

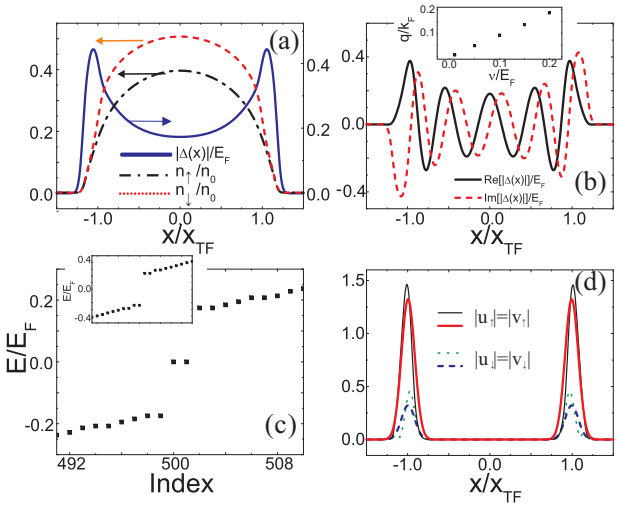

FIG. 1: (a) Density profiles $n_\sigma(x)$ in units of n_0 (left y-axis) and order parameter profile $|\Delta(x)|$ in units of E_F (right y-axis). (b) The real and imaginary parts of the order parameter profile. The inset shows the pairing momentum q as a function of ν. (c) Low-lying spectrum of quasi-particle excitation. The inset shows the corresponding spectrum of a topologically trivial phase with $\nu = 0$ and $h = 0.5E_F$ with other parameters the same as those of the rest of the figure. (d) Wavefunction of the Majorana modes. The thin (thick) lines represent numerical (analytical) results. The parameters used for this figure are $\gamma = 2.2$, $\lambda = 1.5E_F/k_F$, $h = 0.8E_F$, and $\nu = 0.2E_F$ unless otherwise noted.

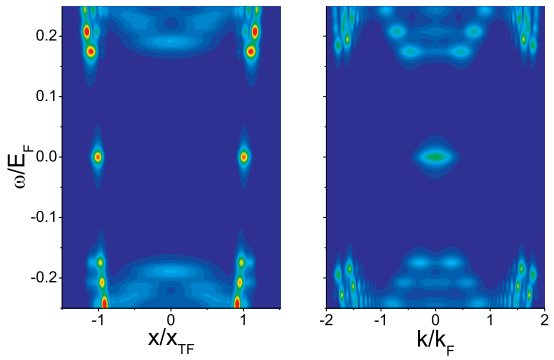

FIG. 2: Density of states in real space (left panel) and in momentum space (right panel). The parameters are the same as in Fig. 1. Brighter color represents higher density of states.

the linearization of the BdG Hamiltonian around $x = x_0$ and $k = 0$, where x_0 is a real-space position near which the Majorana modes are localized. A natural choice for x_0 is inspired by the local density approximation at this point. The local, homogeneous Hamiltonian becomes topologically nontrivial, has zero eigenvalues when the Zeeman field strength $b = \sqrt{h^2 + \nu^2}$ exceeds the critical value $\sqrt{\mu^2(x_0) + |\Delta(x_0)|^2}$, where $\mu(x) = \mu - V_T(x)$. Hence we choose x_0 such that $b = \sqrt{\mu^2(x_0) + |\Delta(x_0)|^2}$.

Neglecting the kinetic energy term, approximating $V_T(x)$ by $\frac{1}{2}m\omega^2 x_0^2 + m\omega^2 x_0(x - x_0)$, and replacing $\Delta(x)$ by $\Delta(x_0) \equiv \Delta_0$ leads to a linearized $H_{\rm BdG}$. The zero energy modes of the linearized $H_{\rm BdG}$ are found by using degenerate perturbation theory and leads to Majorana modes that are Gaussians localized at either left or right edge of the harmonic trap and given by

$$|L, R\rangle = \frac{e^{-\frac{(x-x_0)^2}{2\sigma^2}}}{\sqrt[4]{\pi\sigma^2}}\chi \quad \text{and} \quad \sigma^2 = \frac{\sqrt{|\Delta_0|^2 - \nu^2}}{\sqrt{b^2 - |\Delta_0|^2}}\frac{\lambda}{|m\omega^2 x_0|} ,$$

where $|L, R\rangle$ are the left/right localized edge states, χ is a spatially independent Nambu function given in the Supplemental Material [46]. We plot the analytical wavefunctions of the Majorana modes in Fig. 1(d) together with the numerical results. The agreement is remarkable.

Expansion of the FF state — The characteristic signature of the FF state is finite-momentum pairing. Here, we show how this feature manifests itself in the density profiles of the atomic cloud during time-of-flight expansion. Figure 3 shows the time evolution of the density profiles for both an interacting and a non-interacting gas. Initially, the density profiles of both spin states are symmetric about the trap center. As the cloud expands, the profiles become asymmetric when $\nu \neq 0$. Furthermore, the center of mass of each spin state moves in opposite directions regardless of whether the atoms interact or not. There is, however, an important difference between an interacting and a non-interacting cloud. As shown in Fig. 4, for a non-interacting cloud, the center-of-mass position of the whole cloud, defined as

$$x_{\rm cm} = \frac{1}{N}\sum_{\sigma=\uparrow,\downarrow}\int x\, n_\sigma(x)\, dx ,$$

remains at zero, while $x_{\rm cm}$ for an interacting cloud deviates from zero as time increases. The deviation is stronger for larger interaction strength γ and larger in-plane Zeeman field strength $|\nu|$. This result is consistent with a two-body calculation carried out by Dong *et al.* [19], where they found that the total mechanical momentum of the interaction-induced two-body bound state becomes finite as long as the in-plane Zeeman field is present. In the present study, the non-zero $x_{\rm cm}$ during the expansion is a direct consequence of the finite-momentum FF pairing in the original trapped system. That $x_{\rm cm}$ changes faster for larger interaction strength can be attributed to stronger pairing, and hence a larger fraction of the atoms form Cooper pairs with finite momentum.

Conclusion — We have considered both the static and dynamical properties of a trapped 1D Fermi gas subject to equal-weight Rashba-Dresselhaus spin-orbit coupling. This system enters an exotic topological FF state regime when a large effective Zeeman field with a non-zero in-plane component is present. The two salient features of this phase is (1) the presence of zero-energy Majorana modes localized near the edge of the trap; and (2) finite-momentum pairing. These features manifest themselves in the density of states and the center-or-mass displacement during expansion, respectively. We hope future experiments may be able to realize and probe this interesting quantum phase.

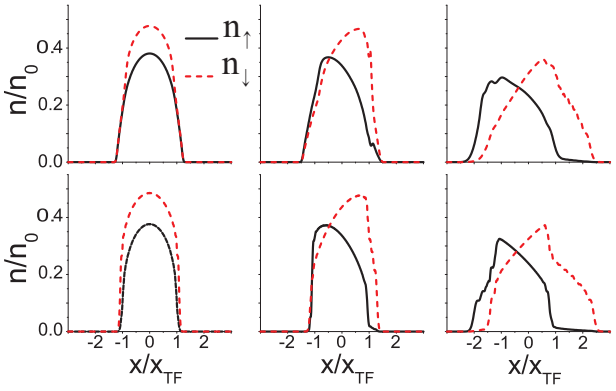

FIG. 3: Expansion dynamics of the Fermi cloud released at time $t = 0$. Top row: A interacting case with $\gamma = 2.2$. Bottom row: A non-interacting case with $\gamma = 0$. Other parameters are: $\lambda = 1.5E_F/k_F$, $h = 0.8E_F$ and $\nu = 0.2E_F$. From left to right are plots of density profiles at $t = 0$, $0.88/\omega_0$, and $2.04/\omega_0$, respectively.

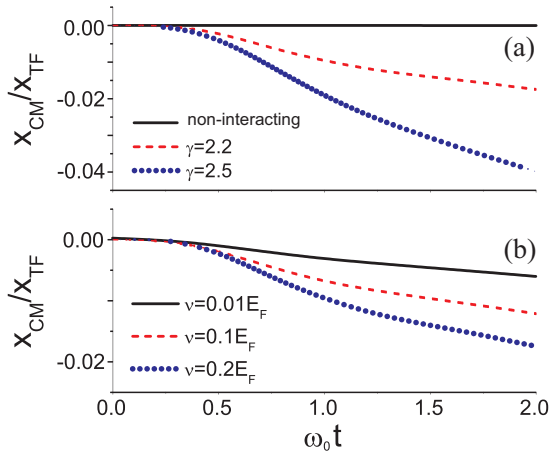

FIG. 4: Center-of-mass position of the atomic cloud during free expansion. In (a), different curves represent different interaction strengths for $\nu = 0.2E_F$. In (b), different curves represent different in-plane Zeeman fields for $\gamma = 2.2$. Other parameters are the same as in Fig. 3.

Acknowledgements — LJ and ET acknowledge support from the US Army Research Office under Contract No. 60661PH. XJL and HH are supported by the ARC Discovery Projects (DP140100637, FT 130100815 and DP140103231). HP is supported by the NSF and the Welch Foundation (Grant No. C-1669). We would like to thank Leslie Baksmaty for useful discussions.

[1] J. D. Sau, R.M. Lutchyn, S. Tewari, and S. Das Sarma, Phys. Rev. Lett. **104**, 040502 (2010).

[2] Y. Oreg, G. Refael, and F. von Oppen, Phys. Rev. Lett. **105**, 177002 (2010).

[3] V. Mourik, K. Zuo, S. M. Frolov, S. R. Plissard, E. P. A. M. Bakkers, and L. P. Kouwenhoven, Science **336**, 1003 (2012).

[4] Y.-J. Lin, K. Jiménez-García, and I. B. Spielman, Nature (London) **471**, 83 (2011).

[5] M. Sato, Y. Takahashi, and S. Fujimoto, Phys. Rev. Lett. **103**, 020401 (2009).

[6] J. P. Vyasanakere, S. Zhang, and V. B. Shenoy, Phys. Rev. B **84**, 014512 (2011).

[7] H. Hu, L. Jiang, X.-J. Liu, and H. Pu, Phys. Rev. Lett. **107**, 195304 (2011).

[8] Z.-Q. Yu, and H. Zhai, Phys. Rev. Lett. **107**, 195305 (2011).

[9] M. Gong, S. Tewari, and C. Zhang, Phys. Rev. Lett. **107**, 195303 (2011).

[10] W. Yi, and G.-C. Guo, Phys. Rev. A **84**, 031608(R) (2011).

[11] M. Iskin, and A. L. Subaşi, Phys. Rev. Lett. **107**, 050402 (2011).

[12] L. Han, and C. A. R. Sá de Melo, Phys. Rev. A **85**, 011606(R) (2012).

[13] P. Wang, Z.-Q. Yu, Z. Fu, J. Miao, L. Huang, S. Chai, H. Zhai, and J. Zhang, Phys. Rev. Lett. 109 , 095301 (2012).

[14] L. W. Cheuk, A. T. Sommer, Z. Hadzibabic, T. Yefsah, W. S. Bakr, and M. W. Zwierlein, Phys. Rev. Lett. 109 , 095302 (2012).

[15] Xia-Ji Liu and Hui Hu, Phys. Rev. A **85**, 033622 (2012).

[16] Xia-Ji Liu and Peter D. Drummond, Phys. Rev. A **86**, 035602 (2012).

[17] Ran Wei and Erich J. Mueller, Phys. Rev. A **86**, 063604 (2012).

[18] Takeshi Mizushima and Masatoshi Sato, New J. Phys. **15**, 075010 (2013).

[19] Lin Dong, Lei Jiang, Hui Hu, and Han Pu, Phys. Rev. A **87**, 043616 (2013).

[20] Lin Dong, Lei Jiang, and Han Pu, New J. Phys. **15**, 075014 (2013).

[21] V. B. Shenoy, Phys. Rev. A **88**, 033609 (2013).

[22] Z. Zheng, M. Gong, X. Zou, C. Zhang, and G.-C. Guo, Phys. Rev. A **87**, 031602(R) (2013).

[23] F. Wu, G.-C. Guo, W. Zhang, and W. Yi, Phys. Rev. Lett. **110**, 110401 (2013).

[24] Xia-Ji Liu and Hui Hu, Phys. Rev. A **87**, 051608(R) (2013).

[25] Xia-Ji Liu and Hui Hu, New J. Phys. **15**, 093037 (2013).

[26] Chunlei Qu, Zhen Zheng, Ming Gong, Yong Xu, Li Mao, Xubo Zou, Guangcan Guo and Chuanwei Zhang, Nature Commun. **4**, 2710 (2013).

[27] Wei Zhang and Wei Yi, Nature Commun. **4**, 2711 (2013).

[28] Xia-Ji Liu and Hui Hu, Phys. Rev. A **88**, 023622 (2013).

[29] Chun Chen, Phys. Rev. Lett. **111**, 235302 (2013).

[30] J. Ruhman and E. Altman, arXiv:1401.7343.

[31] M. W. Zwierlein, A. Schirotzek, C. H. Schunck, and W. Ketterle, Science **311**, 492 (2006).

[32] G. B. Partridge, W. Li, R. I. Kamar, Y.-A. Liao, and R. G. Hulet, Science **311**, 503 (2006).

[33] S. Nascimbene, N. Navon, K. J. Jiang, L. Tarruell, M. Teichmann, J. McKeever, F. Chevy, and C. Salomon, Phys. Rev. Lett. 103, 170402 (2009).

[34] Y.-A. Liao, A. S. C. Rittner, T. Paprotta, W. Li, G. B. Partridge, R. G. Hulet, S. K. Baur, and E. J. Mueller, Nature (London) 467, 567 (2010).

[35] B. Sundar and E. J. Mueller, Phys. Rev. A **88**, 063632 (2013).

[36] Xia-Ji Liu, Hui Hu, and Peter D. Drummond, Phys. Rev. A **76**, 043605 (2007).

[37] Daniel T. Colbert and William H. Miller, J. Chem. Phys. 96, 1982 (1992).

[38] Xia-Ji Liu, Phys. Rev. A **87**, 013622 (2013).

[39] G. Tonini, F. Werner, and Y. Castin, Eur. Phys. J. D **39**, 283 (2006).

[40] K. J. Challis, R. J. Ballagh, and C. W. Gardiner, Phys. Rev. Lett. 98, 093002 (2007).

[41] R. G. Scott, F. Dalfovo, L. P. Pitaevskii, and S. Stringari , Phys. Rev. Lett. 106, 185301 (2011).

[42] Hong Lu, L. O. Baksmaty, C. J. Bolech, and Han Pu, Phys. Rev. Lett. **108**, 225302 (2012).

[43] P. Fulde and R. A. Ferrell, Phys. Rev. 135 , A550 (1964).

[44] A. I. Larkin and Y. N. Ovchinnikov, Zh. Eksp. Teor. Fiz. 47 , 1136 (1994) [Sov. Phys. JETP 20 , 762 (1965)].

[45] Lei Jiang, Leslie O. Baksmaty, Hui Hu, Yan Chen, and Han Pu, Phys. Rev. A 83, 061604(R) (2011).

[46] See Supplemental Material for details on the analytic derivation of Majorana wavefunctions.

arXiv:1404.6211v1 [cond-mat.quant-gas] 24 Apr 2014

Supplemental Material

Lei Jiang[1], Eite Tiesinga[1], Xia-Ji Liu[2], Hui Hu[2] and Han Pu[3]
[1] *Joint Quantum Institute, University of Maryland and National Institute of Standards and Technology, Gaithersburg, Maryland 20899, USA*
[2] *Centre for Atom Optics and Ultrafast Spectroscopy, Swinburne University of Technology, Melbourne 3122, Australia*
[3] *Department of Physics and Astronomy, and Rice Quantum Institute, Rice University, Houston, Texas 77251, USA*
(Dated: April 25, 2014)

In this Supplemental Material, we provide details on how to derive the analytic wavefunction of the Majorana modes for a trapped 1D system. Our method relies on a linearization of the Bogoliubov-de Gennes (BdG) Hamiltonian based on the fact that Majorana modes are localized in both real (near the trap edges) and momentum (near zero momentum) space. We divide the BdG Hamiltonian $H_{\rm BdG} = H_0 + H_1 + H_2$, where H_0, a local Hamiltonian at real-space point x_0 near which the Majorana modes are localized, is given by

$$H_0 = \begin{pmatrix} \frac{1}{2}m\omega^2 x_0^2 - \mu - h & -i\nu & 0 & -\Delta_0 \\ i\nu & \frac{1}{2}m\omega^2 x_0^2 - \mu + h & \Delta_0 & 0 \\ 0 & \Delta_0^* & -\frac{1}{2}m\omega^2 x_0^2 + \mu + h & -i\nu \\ -\Delta_0^* & 0 & i\nu & -\frac{1}{2}m\omega^2 x_0^2 + \mu - h \end{pmatrix},$$

H_1 contains the linearized potential and spin-orbit coupling term given by

$$H_1 = \begin{pmatrix} m\omega^2 x_0(x-x_0) & -i\lambda\hat{k} & 0 & 0 \\ i\lambda\hat{k} & m\omega^2 x_0(x-x_0) & 0 & 0 \\ 0 & 0 & -m\omega^2 x_0(x-x_0) & i\lambda\hat{k} \\ 0 & 0 & -i\lambda\hat{k} & -m\omega^2 x_0(x-x_0) \end{pmatrix}.$$

Finally, H_2 contains the kinetic energy and corrections of the order parameter $\Delta(x)$ near $\Delta_0 \equiv \Delta(x_0)$. We neglect H_2 in our calculation.

The local Hamiltonian H_0 has two degenerate zero-energy states when

$$b = \sqrt{\left(\frac{1}{2}m\omega^2 x_0^2 - \mu\right)^2 + |\Delta_0|^2},$$

where the effective Zeeman field strength $b = \sqrt{h^2+\nu^2}$ combines both the in- and out-of-plane field. This equation sets the value of x_0. In our parameter region, x_0 has two solutions $\pm|x_0|$, localized near the left and right edge of the harmonic trap, respectively. The corresponding zero-energy eigenstates are

$$\begin{aligned} |1\rangle &= \left(-\frac{a+h}{\sqrt{2b^2+2ah}}, \frac{i\nu}{\sqrt{2b^2+2ah}}, 0, \frac{\Delta_0^*}{\sqrt{2b^2+2ah}}\right)^T, \\ |2\rangle &= \left(\frac{i\nu}{\sqrt{2b^2-2ah}}, \frac{a-h}{\sqrt{2b^2-2ah}}, \frac{\Delta_0^*}{\sqrt{2b^2-2ah}}, 0\right)^T, \end{aligned}$$

where $a = \sqrt{b^2 - |\Delta_0|^2}$. The two other eigenstates of H_0 have finite energy $\pm 2b$. As we are only interested in zero-energy states of the Hamiltonian, we neglect the effects of these two energy states in the following.

Next, we treat H_1 as a small perturbation to H_0 in the subspace spanned by $\{|1\rangle, |2\rangle\}$. In this two dimensional subspace, H_1 takes the form

$$H_1^{\rm eff} = \begin{pmatrix} \frac{a(a+h)}{b^2+ah}\tau\hat{x} - \frac{(a+h)\nu}{b^2+ah}\lambda\hat{k}, & -\frac{a\nu}{\sqrt{b^4-a^2h^2}}i\tau\hat{x} + \frac{\nu^2-|\Delta_0|^2}{\sqrt{b^4-a^2h^2}}i\lambda\hat{k} \\ \frac{a\nu}{\sqrt{b^4-a^2h^2}}i\tau\hat{x} - \frac{\nu^2-|\Delta_0|^2}{\sqrt{b^4-a^2h^2}}i\lambda\hat{k}, & \frac{a(a-h)}{b^2-ah}\tau\hat{x} - \frac{(a-h)\nu}{b^2-ah}\lambda\hat{k} \end{pmatrix},$$

where $\tau = m\omega^2 x_0$ and $\hat{x} = x - x_0$.

In real space, the momentum operator takes the form $\hat{k} = -id/dx$ and we search for a zero-energy eigenstate $(p, q)^T$ of $H_1^{\rm eff}$. This leads to coupled differential equations for p and q with unit-normalized Gaussian solutions

$$\begin{aligned} p &= \frac{1}{\sqrt[4]{\pi\sigma^2}} e^{-\frac{(x-x_0)^2}{2\sigma^2}}, \\ q &= -\mathrm{sgn}(\tau)\sqrt{\frac{h+a}{h-a}}\sqrt{\frac{b^2-ah}{b^2+ah}}\, p, \end{aligned}$$

where $\mathrm{sgn}(z)$ is the sign of z and the width σ is determined by $\sigma^2 = \lambda\sqrt{h^2-a^2}/(|\tau|a)$. The two corresponding normalized Nambu wavefunctions are

$$|L,R\rangle = [u_\uparrow(x), u_\downarrow(x), v_\uparrow(x), v_\downarrow(x)]^T = \frac{1}{\sqrt[4]{\pi\sigma^2}}\, e^{-\frac{(x-x_0)^2}{2\sigma^2}}\, \chi_{L,R},$$

with

$$\chi_{L,R} = \left(\frac{-\sqrt{h+a}[\sqrt{h^2-a^2} + \mathrm{sgn}(\tau) i\nu]}{2\sqrt{h}|\Delta_0|}, \frac{\sqrt{h-a}[i\nu + \mathrm{sgn}(\tau)\sqrt{h^2-a^2}]}{2\sqrt{h}|\Delta_0|}, -\mathrm{sgn}(\tau)\frac{\sqrt{h+a}}{2\sqrt{h}}\frac{\Delta_0^*}{|\Delta_0|}, \frac{\sqrt{h-a}}{2\sqrt{h}}\frac{\Delta_0^*}{|\Delta_0|} \right)^T,$$

where the left and right localized edge states $|L,R\rangle$ require $\mathrm{sgn}(\tau) = -1$ and 1, respectively. One can check that the wavefunctions satisfy the symmetry requirement $|u_\sigma| = |v_\sigma|$ for Majorana modes. Finally, in order to compare with numerical results of our self-consistent BdG calculations, we define the symmetric and anti-symmetric states $|\varphi^\pm\rangle = (|L\rangle \pm |R\rangle)/\sqrt{2}$.

In deriving the above results, we have assumed that $\nu < |\Delta_0|$. This is reasonable as for large ν the order parameter becomes vanishingly small. In the limit $\nu \ll |\Delta_0|$, the wavefunction of the Majorana mode takes the form

$$|L,R\rangle = \frac{1}{\sqrt[4]{\pi\sigma^2}} e^{-\frac{(x-x_0)^2}{2\sigma^2}} \left(\frac{-(a+h)}{2\sqrt{h^2+ah}}, \mathrm{sgn}(\tau)\frac{(h-a)}{2\sqrt{h^2-ah}}, -\mathrm{sgn}(\tau)\frac{\Delta_0^*}{2\sqrt{h^2-ah}}, \frac{\Delta_0^*}{2\sqrt{h^2+ah}} \right)^T.$$

[1] Ran Wei and Erich J. Mueller, Phys. Rev. A **86**, 063604 (2012).